ACS Energy LETTERS

http://pubs.acs.org/journal/aelccp

Inelastic Deformation in Methylammonium Lead Iodide Perovskite and Mitigation by Additives during Thermal Cycling

Anton A. Samoylov, Matthew Dailey, Yanan Li, Patrick J. Lohr, Sean Raglow, and Adam D. Printz*

Cite This: *ACS Energy Lett.* 2024, 9, 2101−2108

Read Online

ACCESS | Metrics & More | Article Recommendations | Supporting Information

ABSTRACT: Metal halide perovskite thin films are promising materials for next-generation photovoltaic applications, but the thermomechanical instabilities of these materials are critical barriers to device longevity. In this study, we measure the evolution of stresses in methylammonium lead iodide ($MAPbI_3$) films thermally cycled from 25 to 105 °C using a multibeam optical stress sensor (MOSS) system. We demonstrate that these films undergo residual stress buildup due to inelastic deformation as well as a simple mitigation strategy by incorporating low concentrations of 5-aminovaleric acid hydrochloride (5-AVACl) as an additive. Adding 5-AVACl increases the tensile stresses measured at room temperature but beneficially decreases the biaxial modulus from 9.60 ± 0.44 GPa to 7.95 ± 0.55 GPa, resulting in greater accommodation of thermal stresses. The hysteresis loop is ∼63% smaller with the inclusion of 5-AVACl, and the stress relaxation at 50 °C decreases from 86.46 to 51.49 MPa. The larger stress relaxation in pristine $MAPbI_3$ is correlated with grain boundary opening after five cycles, while the inclusion of 5-AVACl mitigates this degradation. Our findings underscore the importance of studying the dynamic response of perovskite films during thermal cycling and lay the foundation for further exploration into the mechanisms governing the thermomechanical behavior of perovskite thin films.

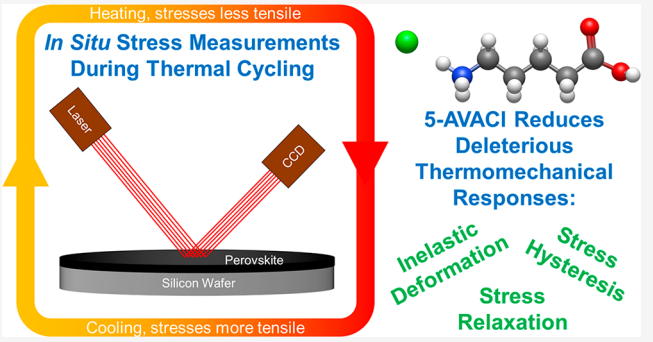

Metal halide perovskites ("perovskites") are a promising family of next-generation semiconducting materials, frequently demonstrated in photovoltaic (PV) applications with power conversion efficiencies (PCEs) comparable to crystalline silicon, but at a fraction of the processing cost and material usage.[1,2] Perovskite-based devices comprise thin films deposited onto substrates that can mechanically constrain the system and impart stresses within the perovskite layers due to coefficient of thermal expansion (CTE)[3] or lattice mismatches.[4] The CTE mismatch can be particularly problematic, as the CTE of perovskites is typically an order of magnitude greater than that of the underlying glass or silicon substrate, resulting in tensile stress buildup in the perovskite as the film is cooled after annealing.[5,6] These stresses have been reported to be high enough to deform copper, which can result in poor mechanical and chemical stability under environmental stressors.[5] Furthermore, residual tensile stresses weaken bonds within the perovskite crystal, resulting in less stable films due to reduced formation energies of defects and activation energies of ion migration.[7−9] Recent reports have described the formation of stresses in perovskite thin films during the fabrication steps[10] and its effect on device performance,[9] but no study of the evolution of stresses during heating and cooling cycles has yet been reported. Given that perovskite-based photovoltaic devices are subjected to daily thermal cycling during operation, it is critically important to understand the stress evolution during thermal cycling in perovskite films.

While *in situ* stress measurements of perovskite thin films during thermal cycling have not yet been reported, the influence of thermal cycling on stresses in other materials such as copper (Cu) thin films has been extensively studied.[11,12] In Cu films, stress responses during thermal cycling and complementary isothermal stress relaxation experiments have been correlated with film voiding and increased electrical

Received: February 27, 2024
Revised: April 5, 2024
Accepted: April 9, 2024
Published: April 11, 2024

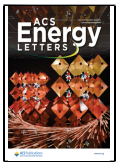

https://doi.org/10.1021/acsenergylett.4c00587
ACS Energy Lett. 2024, 9, 2101−2108

resistance and reduced reliability.[13,14] Unlike copper, metal halide perovskite thin films exhibit phase transitions—e.g., the tetragonal to cubic transformation in $MAPbI_3$ that occurs at ~54 °C—and ferroelasticity that can contribute to much more mechanistically complex stress−strain behaviors.[15−20]

Residual stresses in thin films are frequently measured as instantaneous responses, but these stresses induce time-dependent mechanical deformation or creep. During thermal cycling, stresses can change rapidly without reaching their steady state, making deformation mechanisms difficult to study.[11,21] However, deformation mechanisms can be better understood using isothermal measurements to measure, for example, time-dependent stress relaxation.[22−24] These stress-relaxation behaviors can then be fit to models such as power law or diffusional creep to gain insight into the dominant deformation mechanisms a thin film experiences at given temperatures and stresses.[11,25,26] Since the aforementioned creep models were developed for crystalline solids, similar approaches can be explored for perovskite films to assess the dominant deformation mechanisms being experienced.

In this work, we aimed to understand how stresses in metal halide perovskite films evolve under dynamic thermal conditions, as well as stress responses to isothermal conditions. For this initial study, we selected $MAPbI_3$, because it is a well-characterized perovskite and has relative compositional simplicity. We used a multibeam optical stress sensor (MOSS) to determine the stresses in the metal halide perovskite films on silicon (Figure 1). In MOSS measurements, an array of laser beams is reflected off the surface of interest and the distance between the reflected beams is measured at the detector to determine the radius of curvature, which can be correlated to stresses through Stoney's equation:[27−29]

$$\sigma = \frac{E_s}{1-\nu_s}\frac{t_s^2}{6t_f}\left(\frac{1}{R}-\frac{1}{R_0}\right) \quad (1)$$

where E_s is the Young's modulus of the substrate, ν_s is the Poisson's ratio of the substrate, t_s and t_f are the thicknesses of the substrate and thin film, R is the radius of curvature of the substrate with the thin film deposited on top, and R_0 is the radius of curvature of the bare substrate. In the case of a perovskite film facing upward—i.e., the laser beams are reflected off the perovskite rather than the substrate—under tensile stresses, the film pulls the substrate into a concave curvature and the laser beams move closer together at the detector. Under compressive stresses, the substrate curvature is more convex, and the laser beams move farther apart.

The biaxial stresses for the first two thermal cycles of pristine $MAPbI_3$ films are shown in Figure 2. As the films are heated, an initial decrease in stress—i.e., the stress was less tensile (positive value) or more compressive (negative value)—was observed. This initial decrease in the stresses was linear and associated with elastic stress−strain response.[3,30] With continued heating, the stresses reached a minimum and then began to increase either significantly (~60 °C for the first cycle) or slowly (~80 °C for subsequent cycles), which was associated with the rate of plastic relaxation exceeding the stress loading rate.[13] At the initiation of the cooling cycle, the films underwent an elastic increase in stresses, which then gave way to inelastic deformation below 95 °C.

During the first thermal cycle, stress buildup was observed after the cooling cycle—i.e., the film stress after the first thermal cycle was greater than the initial film stress. This loop opening upon the first cycle was previously observed in other thin film materials such as copper and was attributed to plastic yielding occurring within the film, primarily from grain growth

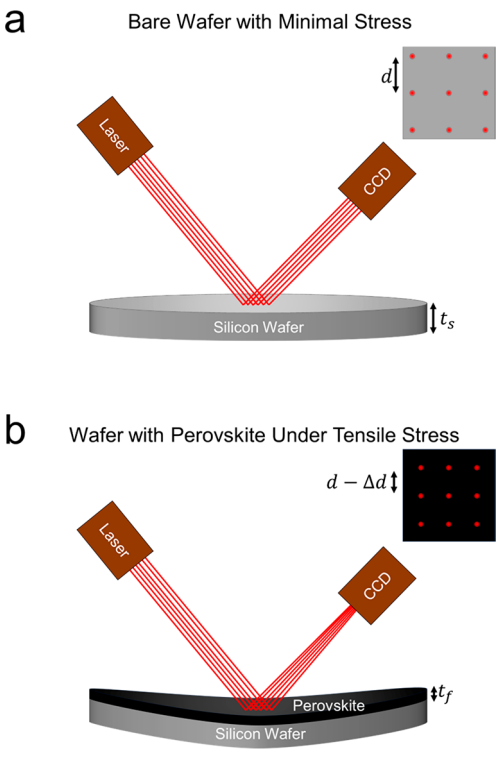

Figure 1. Schematic of the multibeam optical stress sensor (MOSS) measuring curvature. (a) On a bare wafer, there will be minimal stress, and curvature is expected to be low. The laser beam array at the detector has a spacing of *d*. (b) Typically, a perovskite film on top of a wafer undergoes tensile stresses, which will result in a slight concave curvature of the wafer. This curvature will result in the laser beams reaching the detector at a closer distance, $d - \Delta d$.

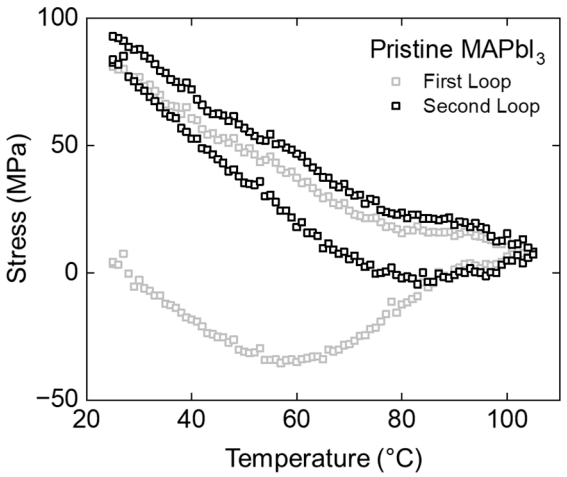

Figure 2. Biaxial stresses during two thermal cycles for pristine $MAPbI_3$. The first cycle is an "open loop" with crystal reorganization or grain growth likely occurring. The second (and subsequent) cycles have stabilized hysteresis loops, where the stresses at 25 °C before and after the thermal cycle are essentially identical.

https://doi.org/10.1021/acsenergylett.4c00587
ACS Energy Lett. 2024, 9, 2101−2108

and the elimination of grain boundaries.[3,12] For the pristine $MAPbI_3$ films, an initial jump of 83 ± 11 MPa was seen in the first heating−cooling cycle. In subsequent cycles, the stress buildup was much smaller but still present in pristine $MAPbI_3$ at 25 °C (Figures S1 and S2). In thin film Cu systems, such "open loop" hysteresis is undesirable due to potential void formation when the deposited Cu is used as interconnect material in electronic circuitry.[13,14] Similar voiding in perovskite has been observed in $MAPbI_3$ under repeated bending, which resulted in poor device operational stability.[31] In $MAPbI_3$, yielding could be due in part to lattice constant hysteresis at the tetragonal to cubic phase transition.[32] During thermal cycling from 315 to 346 K, Arakcheeva and co-workers observed this hysteresis and attributed it to phase modulation—e.g., periodic variation of both pseudocubic and pseudotetragonal regions—which then settled into a thermodynamically stable phase after multiple thermal cycles.[32]

Given that additives have previously been shown to improve the mechanical durability of metal halide perovskites,[31,33−38] we hypothesized that the stress hysteresis in the perovskite films could be mitigated by introducing an organic additive, which could adsorb onto surfaces and potentially relax stresses due to its relatively lower stiffness compared to perovskite. For this study, we used the additive 5-aminovaleric acid hydrochloride (5-AVACl), which we previously showed improved the optoelectronic properties and stability of $MAPbI_3$ films when added in low concentrations.[39] To ensure an appropriate comparison, we fabricated the films with the same processing parameters, resulting in a film thickness of 388 ± 19 nm for pristine $MAPbI_3$ and a film thickness of 406 ± 18 nm for $MAPbI_3$ with 1 mol % 5-AVACl added. With the addition of 1 mol % 5-AVACl, we observed that the stress buildup during the first thermal cycle decreased ∼35% to 53 ± 10 MPa. Furthermore, we observed no stress buildup in the subsequent thermal cycles (Figure S1), indicating improved mechanical stability to thermal cycling compared to pristine $MAPbI_3$.

Interestingly, incorporating 1 mol % 5-AVACl changed the shape of the stabilized hysteresis loops, resulting in a notable decrease in the hysteresis loop area. This decrease in the hysteresis was attributed to reduced inelastic deformation between thermal cycling loops and steep slopes in the elastic regions of the curves (Figure 3). We quantified the change in loop shape by integrating the hysteresis area of the stabilized second loops—i.e., the area between the heating and cooling curves—for pristine $MAPbI_3$ and 5-AVACl containing films. In pristine films, the hysteresis area was 1418 ± 213 MPa-°C, which decreased to 528 ± 212 MPa-°C (a 62.7 ± 26.9% decrease) with the inclusion of 5-AVACl. Furthermore, we observed that during the heating cycles the tensile stresses in pristine $MAPbI_3$ started to increase slightly above ∼80 °C, indicative of high extents of inelastic deformation, while films with 5-AVACl continued to exhibit decreased tensile stresses—which never became compressive—throughout the heating cycle. The reduced inelastic deformation observed in the films with 5-AVACl could possibly be due in part to improved perovskite crystal orientation (Figure S3), which has been shown to lead to lower localized strain in perovskite films.[40] This improvement in crystal orientation was confirmed by grazing incidence wide-angle X-ray scattering (GIWAXS) results, which showed a highly oriented (110) plane at an azimuth angle of 90° when incorporating 5-AVACl into the films, suggesting a preferred orientation parallel to the substrate. In contrast, the pristine $MAPbI_3$ film was only

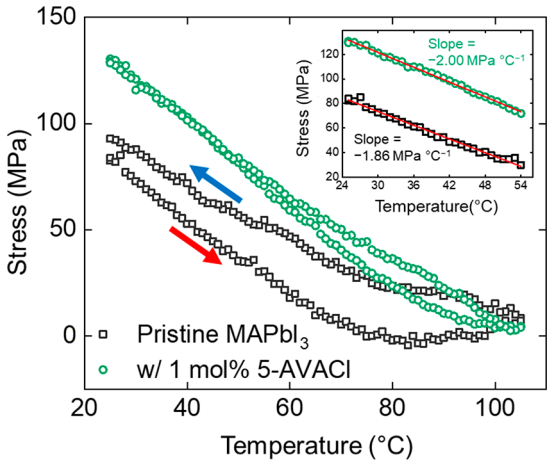

Figure 3. Second thermal cycles (the first stabilized hysteresis loops) for pristine $MAPbI_3$ and $MAPbI_3$ with 1 mol % 5-AVACl. With 5-AVACl, the stresses are higher but the hysteresis is smaller, indicative of a lower extent of plastic deformation. (Inset) Biaxial moduli for these films were calculated using the slope of the curves during the heating cycle in the temperature range with linear elastic behavior (25−54 °C).

partially oriented. Moreover, the introduction of 5-AVACl provided structural flexibility and enhanced the ability of the film to bear the applied stress and lattice distortion, thus improving the lattice stability and mechanical robustness of the perovskite films.[41]

Critically, it should be noted that films with 5-AVACl had higher residual stresses at room temperatures; in previous reports, these higher stresses would be indicative of a material that would likely exhibit poor thermomechanical stability.[5,6] However, the smaller hysteresis observed in these films than in pristine films suggested that absolute stresses are not the most important indicator for the mechanical robustness of thin films—a conclusion supported by previous work studying thermal cycling behavior of unpassivated and passivated copper films.[42]

We also observed different slopes in the linear elastic regions of these stress-temperature curves. The linear elastic regions of the curves can be used to calculate the biaxial moduli of the films according to eq 2:[3]

$$\frac{d\sigma}{dT} = \Delta\alpha\left[\frac{E}{1-\nu}\right]_f \tag{2}$$

where $\frac{d\sigma}{dT}$ is the slope of the linear elastic region of the heating curve, $\Delta\alpha = \alpha_s - \alpha_f$ is the difference between the coefficients of thermal expansion (CTE) of the substrate (α_s) and film (α_f), and $\left[\frac{E}{1-\nu}\right]_f$ is the biaxial modulus of the film.

The substrates used were Si wafers with a (100) crystallographic orientation, which we assigned an approximate CTE of 3.8×10^{-6} K^{-1}.[43] Upon heating, $MAPbI_3$ undergoes a phase transition at 54 °C from tetragonal to cubic, and these two phases have slightly different CTEs. Previous reports have calculated the CTE of the tetragonal phase as 6.1×10^{-5} K^{-1},[9] and of the cubic phase as 4.8×10^{-5} K^{-1}.[44] Furthermore, since much of the linear elastic behavior in the stress loops was below the tetragonal to cubic phase transition, we calculated the biaxial moduli of the tetragonal phase of these films using the tetragonal phase CTE of 6.1×10^{-5} K^{-1}. Given that the 3D

https://doi.org/10.1021/acsenergylett.4c00587
ACS Energy Lett. 2024, 9, 2101−2108

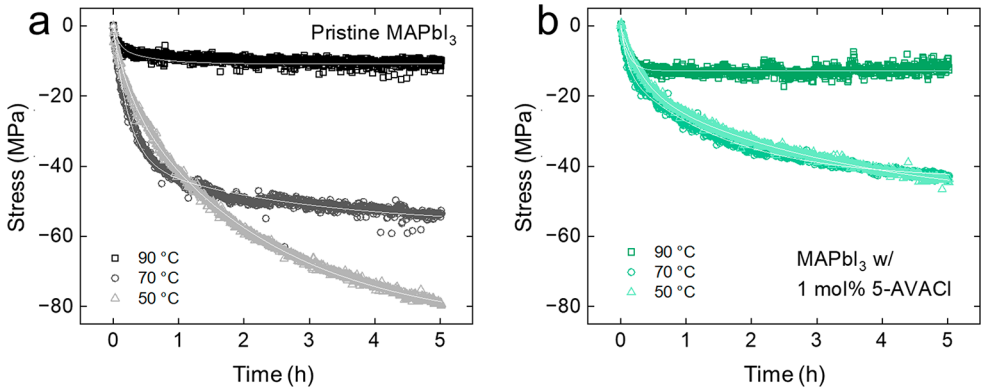

Figure 4. Isothermal stress relaxation for thin films of (a) pristine $MAPbI_3$ and (b) $MAPbI_3$ with 1 mol % 5-AVACl. Biexponential curves were fitted to normalized stress relaxation curves to calculate the relaxation constants. The addition of 5-AVACl decreased the stress relaxation at 50 and 70 °C.

Table 1. Fitting Parameters for Biexponential Modeling of the Isothermal Stress Relaxation for Pristine and 1 mol % 5-AVACl Films

Temp (°C)	Additive	$\Delta\sigma_\infty$ (MPa)	$\Delta\sigma_1$ (MPa)	τ_1 (h)	$\Delta\sigma_2$ (MPa)	τ_2 (h)	R^2
90	None	−10.84	6.72	0.077	4.95	0.531	0.867
	5-AVACl	−12.81	11.16	0.121	1.28	0.121	0.774
70	None	−56.96	38.56	0.231	19.02	2.57	0.996
	5-AVACl	−43.62	13.46	0.103	30.55	1.61	0.993
50	None	−86.46	15.68	0.273	68.75	2.31	0.999
	5-AVACl	−51.49	16.92	0.330	34.89	3.31	0.996

perovskite crystal structure of $MAPbI_3$ was not expected to change significantly with the inclusion of low concentrations of bulky, surface passivating additives, we made the simplifying assumption that the CTEs and phase transition temperature for the perovskite with 5-AVACl were the same as those of pristine $MAPbI_3$ perovskite.

We used the stress−temperature curves of the stabilized second cycles to calculate the slopes, focusing on the linear elastic region from 25 to 54 °C (Figure 3). For pristine $MAPbI_3$, we calculated the biaxial modulus of the tetragonal phase, $E'_{\text{tetra,pristine}}$ to be 9.60 ± 0.44 GPa. For films with 5-AVACl, we calculated $E'_{\text{tetra,5-AVACl}}$ to be 7.95 ± 0.55 GPa, indicating that even at low concentrations the inclusion of additives reduced the stiffness of the perovskite. These moduli were slightly lower than previously reported moduli for single crystalline[45] and thin film[46] perovskite, but still reasonably close.

To determine the method of deformation within the perovskite films, isothermal stress relaxation measurements of the films were performed under an inert N_2 atmosphere for 5 h. Critically, lower extents of stress relaxation have been correlated with more mechanically robust thin films due to their ability to withstand continually applied strain.[21] The films were first cycled from 25−105 °C to stabilize the hysteresis curve and then cycled back up to 105 °C before terminating the thermal cycle on the cooling step at the chosen temperatures of either 50, 70, or 90 °C (Figure 4). It was important to go through this first thermal cycle to stabilize the film microstructure before investigating the effects of steady state temperatures.[21] In this initial study, we approximated stress relaxation behavior with a diffusional creep model based on previously reported isothermal experiments of Cu films initiated from the cooling curves.[11,21] We chose the diffusional model for fitting our perovskite films by assuming that our films had sufficiently fine grains,[25] and that they were cycled under moderate temperatures.[21] We modeled the stress relaxation using a biexponential description shown in eq 3:[11,21]

$$\sigma = \Delta\sigma_\infty + \Delta\sigma_1 \exp\left(-\frac{t}{\tau_1}\right) + \Delta\sigma_2 \exp\left(-\frac{t}{\tau_2}\right) \quad (3)$$

where τ_1 (fast) and τ_2 (slow) are the stress relaxation constants of the isothermal curve, $\Delta\sigma_\infty$ is the zero-creep stress, $\Delta\sigma_1$ and $\Delta\sigma_2$ are the relaxed stress constants, and t is the time variable in hours. The biexponential model fits for the isothermal relaxations are plotted on top of the raw data in Figure 4 and the constants for fitting are given in Table 1. The adjusted R^2 values of the models for the 50 and 70 °C isothermal relaxations were all higher than 0.993; the adjusted R^2 values were lower at 90 °C, but still above 0.77. We attributed the relatively poorer fits at the higher temperature to the lower signal-to-noise ratio due to the smaller magnitudes of stress relaxation.

At 90 °C, the $\Delta\sigma_\infty$ for pristine $MAPbI_3$ was −10.84 MPa and for $MAPbI_3$ with 5-AVACl was −12.81 MPa, indicating that the stress relaxation at low stresses were similar. However, at lower temperatures where film stresses were higher (Figure 3), inclusion of 5-AVACl greatly reduced the amount of stress relaxation, again indicating a more mechanically robust film. At 70 °C, $\Delta\sigma_\infty$ was −56.96 MPa for pristine $MAPbI_3$ and only −43.62 MPa for $MAPbI_3$ with 5-AVACl. At 50 °C, the effect was even more profound with a $\Delta\sigma_\infty$ of −86.46 MPa for pristine $MAPbI_3$ and only −51.49 MPa for $MAPbI_3$ with 5-AVACl. The mechanisms driving the fast and slow relaxations are not at present understood and require further study to differentiate in the future.[21]

We anticipated that the inelastic behavior of these films would result in an observable evolution of the film morphology. As an example, plastic deformation has been

https://doi.org/10.1021/acsenergylett.4c00587
ACS Energy Lett. 2024, 9, 2101−2108

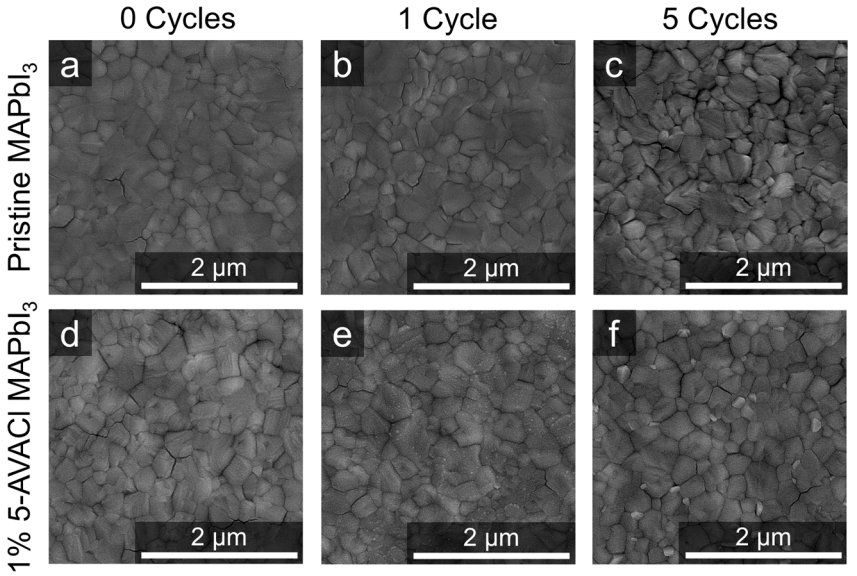

Figure 5. Top-down SEM micrographs of $MAPbI_3$ films at various stages of thermal cycling. (a–c) Pristine $MAPbI_3$ and (d–f) $MAPbI_3$ with 1 mol % 5-AVACl. $MAPbI_3$ film grains remained relatively unchanged (a) before and (b) after one thermal cycle but showed noticeable grain deterioration after (c) five cycles. (d) $MAPbI_3$ films with 5-AVACl showed no visible degradation after (e) one thermal cycle. (f) Possible crystal reorientation was observed after five cycles.

correlated with stress-induced voiding during thermal cycling in copper films due to microstructural transitions from grain growth, crystallinity, and changes to film stress.[22,30,47] In copper, these microstructural transitions drive recrystallization, which occurs over multiple thermal cycles, with the first thermal cycle resulting in residual stress buildup attributed to grain growth, followed by stress loop stabilization in subsequent cycles.[30,47] Another possible mechanism for the loop stabilization could be interfacial reorganization, which has been demonstrated in perovskites with the addition of ammonium salts.[42] We took scanning electron microscope (SEM) micrographs of films before thermal cycling, after the first cycle with the initial residual stress buildup, and after the fifth cycle with stabilized stress loops to qualitatively assess any changes in grain shape or size (Figure 5). In the pristine $MAPbI_3$ films, the films were mostly unchanged after one cycle, but then exhibited signs of degradation resulting in enlarged grain boundaries after five cycles (Figure 5a–c). Conversely, the grains in films with 5-AVACl appeared more resilient after five thermal cycles; however, an emergence of smaller crystals on the film surface appeared after one thermal cycle and continued to grow with additional cycling (Figure 5d–f). The large difference between film morphologies with continued cycling despite stabilized stress responses (Figure S1) was attributed to thermal degradation of the perovskite surface under continued cycling. Further investigation is necessary to determine what these small crystals are, but we did not observe a PbI_2 peak with X-ray diffraction (XRD) after thermal cycling (Figures S4 and S5). Additional conclusions about how the crystallinity might change during thermal cycling require *in situ* grazing incidence X-ray diffraction experiments that were beyond the scope of this initial study.

We used atomic force microscopy (AFM) to determine whether the observed changes in SEM correlated with changes in roughness (Figure S6). The pristine perovskite exhibited a small increase in surface roughness from 17.4 ± 1.5 nm initially to 21.8 ± 1.5 nm after five cycles. The 5-AVACl films exhibited a small decrease in roughness after the initial thermal cycle, decreasing from 22.9 ± 2.5 nm to 18.5 ± 0.7 nm; however, after five cycles the roughness increased to 20.0 ± 0.9 nm, which was consistent with the growth of the small surface crystals observed in SEM. In *ex situ* steady-state photoluminescence (PL), we also observed decreasing peak intensities (Figure S7a, Table S1) with thermal cycling in both pristine and 5-AVACl films, which could be associated with increased defect density.[31,34,48] While a decrease in maximum PL intensity was observed in both pristine $MAPbI_3$ and $MAPbI_3$ with 5-AVACl after five thermal cycles, the decrease was twice as large for pristine $MAPbI_3$ (~60%) as it was when 5-AVACl was added (~30%). These observations were again consistent with the idea that these additives enhanced the ability of the film to accommodate mechanical stresses, as well as the known effect of improved thermal stability due to defect passivation.[49]

Changes in charge carrier lifetimes were determined by time-resolved PL (Figure S7b,c, Table S2). We observed in pristine $MAPbI_3$ similar $\tau_{2,PL}$ lifetimes before cycling (134 ± 21 ns), after one thermal cycle (130 ± 24 ns), and after five thermal cycles (114 ± 3 ns). Conversely, we observed in $MAPbI_3$ films with 5-AVACl that the $\tau_{2,PL}$ lifetime before cycling (151 ± 29 ns) was lower than that after (212 ± 31 ns) one thermal cycle. The $\tau_{2,PL}$ lifetime after five thermal cycles (169 ± 14 ns) returned to a lifetime similar to that before cycling. The trends in lifetime behavior were a bit surprising, but this effect warrants further study to deconvolute the effects of stress, lattice reconstruction, interfacial reorganization, recrystallization, and surface chemistry.

This work demonstrated that $MAPbI_3$ perovskite thin films inelastically deform during thermal cycling, which can lead to enlarged grain boundaries within just a few thermal cycles. Given that metal halide perovskites are predominantly used in photovoltaic applications, where daily thermal fluctuations can be expected, the thermomechanical behavior of perovskites under dynamic thermal conditions represents an important consideration for material and device design for long operational lifetimes. In the initial thermal cycle from 25 to

https://doi.org/10.1021/acsenergylett.4c00587
ACS Energy Lett. 2024, 9, 2101–2108

105 °C, we observed that $MAPbI_3$ films exhibited an open stress−temperature loop with tensile stress buildup, which we attributed to strong inelastic deformation possibly due to lattice reconstruction, interfacial reorganization, or recrystallization. Subsequent thermal cycles also exhibited inelastic deformation but with a closed, stabilized hysteresis loop.

Notably, we determined that inelastic deformation in the stabilized thermal cycles could be significantly mitigated by incorporating 1 mol % 5-AVACl as an additive, which decreased the stress loop hysteresis, tensile stress buildup, and biaxial modulus in the films. Furthermore, inclusion of 5-AVACl changed the shape of the hysteresis curve by reducing inelastic deformation and exhibiting more elastic behavior relative to pristine $MAPbI_3$ films when the films were heated above 80 °C. The isothermal stress relaxation of these films was observed to be well described by the diffusional creep model. Finally, we note that these improvements in thermomechanical behavior with inclusion of 5-AVACl were coupled with an increase in residual stresses at room temperature, indicating that a single temperature stress measurement cannot accurately predict the thermomechanical behavior of metal halide perovskite thin films. This point is a critical consideration for future design and characterization of thermomechanically robust metal halide perovskites films and devices.

We believe that this area of research is ripe for a much deeper exploration to better understand the inelastic deformation behavior in perovskites. Further work is needed to determine the dominant mechanisms driving the inelastic deformation of these perovskites as well as how the perovskite film compositions and processing influence these stress−temperature behaviors and their effects on device performance and operational lifetime. While we showed that additives can reduce inelastic deformation and hysteresis, it is still unclear what mechanisms drive this beneficial behavior. We also see opportunities to expand our scope to investigate the effects of different film deposition and growth methods on the stress responses during thermal cycling. Additionally, future efforts should study the crystallinity change during thermal cycling, the impact of ancillary device layers on the stress behavior of perovskite thin films during thermal cycling, and the overall effects on device PCE. In conclusion, this work demonstrates a new aspect of thermomechanical stability and performance that should be considered when designing perovskite devices from which long operational lifetimes are expected.

■ ASSOCIATED CONTENT

Supporting Information

The Supporting Information is available free of charge at https://pubs.acs.org/doi/10.1021/acsenergylett.4c00587.

Additional experimental details, materials, and methods, including additional thermal cycling experiments, grazing incidence wide angle scattering spectra of initial materials, additional X-ray diffraction spectra, atomic force micrographs;, and steady-state and time-resolved photoluminescence measurements (PDF)

■ AUTHOR INFORMATION

Corresponding Author

Adam D. Printz − *Department of Chemical and Environmental Engineering and Department of Materials Science and Engineering, University of Arizona, Tucson, Arizona 85721, United States;* orcid.org/0000-0002-5264-7792; Phone: +1 520 626 6769; Email: aprintz@arizona.edu

Authors

Anton A. Samoylov − *Department of Chemical and Environmental Engineering, University of Arizona, Tucson, Arizona 85721, United States;* orcid.org/0000-0002-1846-4888

Matthew Dailey − *Department of Chemical and Environmental Engineering, University of Arizona, Tucson, Arizona 85721, United States*

Yanan Li − *Department of Chemical and Environmental Engineering, University of Arizona, Tucson, Arizona 85721, United States*

Patrick J. Lohr − *Department of Chemical and Environmental Engineering, University of Arizona, Tucson, Arizona 85721, United States*

Sean Raglow − *Department of Physics, University of Arizona, Tucson, Arizona 85721, United States*

Complete contact information is available at: https://pubs.acs.org/10.1021/acsenergylett.4c00587

Author Contributions

A.A.S. and A.D.P. conceived this work. M.D. performed initial characterizations with MOSS. Y.L. helped with XRD and PL analysis. P.J.L. helped with MOSS optimizations. S.R. contributed to revisions. The manuscript was written with contributions from all authors. All authors have read and approved the manuscript.

Notes

The authors declare no competing financial interest.

■ ACKNOWLEDGMENTS

This material is based upon work supported by the National Science Foundation under Grant No. 2237211. This material is additionally based upon work supported by the U.S. Department of Energy's Office of Energy Efficiency and Renewable Energy (EERE) under the Solar Energy Technologies Office Award Number DE-EE0009834. This work was further supported by laboratory startup funds from the University of Arizona. P.J.L. was supported by the financial and in-kind contributions of the Phoenix Chapter of the ARCS Foundation. The authors thank the following user facilities at the University of Arizona. All Park AFM images and data were collected in the W. M. Keck Center for Nano-Scale Imaging in the Department of Chemistry and Biochemistry at the University of Arizona, RRID:SCR_022884. This instrument purchase was partially supported by Arizona Technology and Research Initiative Fund (A.R.S.§15-1648). The powder XRD measurements were performed at the XRD facility in the Department of Chemistry and Biochemistry of the University of Arizona, RRID:SCR_022886, on a Philips PANalytical X'Pert PRO MPD instrument. We acknowledge NASA grants #NNX12AL47G and #NNX15AJ22G and NSF grant #1531243 for funding of the instrumentation in the Kuiper Materials Imaging and Characterization Facility at the University of Arizona.

■ REFERENCES

(1) Snaith, H. J. Present Status and Future Prospects of Perovskite Photovoltaics. *Nat. Mater.* **2018**, *17* (5), 372−376.

(2) Song, Z.; McElvany, C. L.; Phillips, A. B.; Celik, I.; Krantz, P. W.; Watthage, S. C.; Liyanage, G. K.; Apul, D.; Heben, M. J. A Technoeconomic Analysis of Perovskite Solar Module Manufacturing with Low-Cost Materials and Techniques. *Energy Environ. Sci.* **2017**, *10* (6), 1297−1305.
(3) Doerner, M. F.; Nix, W. D. Stresses and Deformation Processes in Thin Films on Substrates. *Critical Reviews in Solid State and Materials Sciences* **1988**, *14* (3), 225−268.
(4) Kim, H.-S.; Park, N.-G. Importance of Tailoring Lattice Strain in Halide Perovskite Crystals. *NPG Asia Mater.* **2020**, *12* (1), 78.
(5) Rolston, N.; Bush, K. A.; Printz, A. D.; Gold-Parker, A.; Ding, Y.; Toney, M. F.; McGehee, M. D.; Dauskardt, R. H. Engineering Stress in Perovskite Solar Cells to Improve Stability. *Adv. Energy Mater.* **2018**, *8* (29), 1802139.
(6) Dailey, M.; Li, Y.; Printz, A. D. Residual Film Stresses in Perovskite Solar Cells: Origins, Effects, and Mitigation Strategies. *ACS Omega* **2021**, *6* (45), 30214−30223.
(7) Boyd, C. C.; Cheacharoen, R.; Leijtens, T.; McGehee, M. D. Understanding Degradation Mechanisms and Improving Stability of Perovskite Photovoltaics. *Chem. Rev.* **2019**, *119* (5), 3418−3451.
(8) Xue, D.-J.; Hou, Y.; Liu, S.-C.; Wei, M.; Chen, B.; Huang, Z.; Li, Z.; Sun, B.; Proppe, A. H.; Dong, Y.; Saidaminov, M. I.; Kelley, S. O.; Hu, J.-S.; Sargent, E. H. Regulating Strain in Perovskite Thin Films through Charge-Transport Layers. *Nat. Commun.* **2020**, *11* (1), 1514.
(9) Zhao, J.; Deng, Y.; Wei, H.; Zheng, X.; Yu, Z.; Shao, Y.; Shield, J. E.; Huang, J. Strained Hybrid Perovskite Thin Films and Their Impact on the Intrinsic Stability of Perovskite Solar Cells. *Sci. Adv.* **2017**, *3* (11), eaao5616.
(10) Guo, B.; Chauhan, M.; Woodward, N. R.; McAndrews, G. R.; Thapa, G. J.; Lefler, B. M.; Li, R.; Wang, T.; Darabi, K.; McGehee, M. D.; Amassian, A. In Situ Stress Monitoring Reveals Tension and Wrinkling Evolutions during Halide Perovskite Film Formation. *ACS Energy Lett.* **2024**, *9*, 75−84.
(11) Hwang, S.-J.; Joo, Y.-C.; Koike, J. Stress Relaxation during Isothermal Annealing in Electroplated Cu Films. *Thin Solid Films* **2008**, *516* (21), 7588−7594.
(12) Chen, K.-W.; Hsu, L.-H.; Huang, J.-K.; Wang, Y.-L.; Lo, K.-Y. A Strategic Copper Plating Method Without Annealing Process. *J. Electrochem. Soc.* **2009**, *156* (10), D448.
(13) Thouless, M. D.; Gupta, J.; Harper, J. M. E. Stress Development and Relaxation in Copper Films during Thermal Cycling. *J. Mater. Res.* **1993**, *8* (8), 1845−1852.
(14) Sekiguchi, A.; Koike, J.; Kamiya, S.; Saka, M.; Maruyama, K. Void Formation by Thermal Stress Concentration at Twin Interfaces in Cu Thin Films. *Appl. Phys. Lett.* **2001**, *79* (9), 1264−1266.
(15) Medjahed, A. A.; Dally, P.; Zhou, T.; Lemaitre, N.; Djurado, D.; Reiss, P.; Pouget, S. Unraveling the Formation Mechanism and Ferroelastic Behavior of MAPbI3 Perovskite Thin Films Prepared in the Presence of Chloride. *Chem. Mater.* **2020**, *32* (8), 3346−3357.
(16) Kennard, R. M.; Dahlman, C. J.; DeCrescent, R. A.; Schuller, J. A.; Mukherjee, K.; Seshadri, R.; Chabinyc, M. L. Ferroelastic Hysteresis in Thin Films of Methylammonium Lead Iodide. *Chem. Mater.* **2021**, *33* (1), 298−309.
(17) Li, J.; Zhu, Y.; Huang, P.-Z.; Fu, D.-W.; Jia, Q.-Q.; Lu, H.-F. Ferroelasticity in Organic−Inorganic Hybrid Perovskites. *European Journal* **2022**, *28* (59), No. e202201005.
(18) Strelcov, E.; Dong, Q.; Li, T.; Chae, J.; Shao, Y.; Deng, Y.; Gruverman, A.; Huang, J.; Centrone, A. CH3NH3PbI3 Perovskites: Ferroelasticity Revealed. *Sci. Adv.* **2017**, *3* (4), No. e1602165.
(19) Wright, A. D.; Volonakis, G.; Borchert, J.; Davies, C. L.; Giustino, F.; Johnston, M. B.; Herz, L. M. Intrinsic Quantum Confinement in Formamidinium Lead Triiodide Perovskite. *Nat. Mater.* **2020**, *19* (11), 1201−1206.
(20) Ambrosio, F.; De Angelis, F.; Goñi, A. R. The Ferroelectric−Ferroelastic Debate about Metal Halide Perovskites. *J. Phys. Chem. Lett.* **2022**, *13* (33), 7731−7740.
(21) Gan, D.; Ho, P. S.; Huang, R.; Leu, J.; Maiz, J.; Scherban, T. Isothermal Stress Relaxation in Electroplated Cu Films. I. Mass Transport Measurements. *J. Appl. Phys.* **2005**, *97* (10), No. 103531.
(22) Harper, J. M. E.; Cabral, C., Jr.; Andricacos, P. C.; Gignac, L.; Noyan, I. C.; Rodbell, K. P.; Hu, C. K. Mechanisms for Microstructure Evolution in Electroplated Copper Thin Films near Room Temperature. *J. Appl. Phys.* **1999**, *86* (5), 2516−2525.
(23) Keller, R.-M.; Baker, S. P.; Arzt, E. Stress−Temperature Behavior of Unpassivated Thin Copper Films. *Acta Mater.* **1999**, *47* (2), 415−426.
(24) Kobrinsky, M. J.; Thompson, C. V.; Gross, M. E. Diffusional Creep in Damascene Cu Lines. *J. Appl. Phys.* **2001**, *89* (1), 91−98.
(25) Gibbs, G. B. Diffusion Creep of a Thin Foil. *Philos. Mag.* **1966**, *13* (123), 589−593.
(26) Thouless, M. D. Effect of Surface Diffusion on the Creep of Thin Films and Sintered Arrays of Particles. *Acta Metallurgica et Materialia* **1993**, *41* (4), 1057−1064.
(27) Sinha, A. K.; Sheng, T. T. The Temperature Dependence of Stresses in Aluminum Films on Oxidized Silicon Substrates. *Thin Solid Films* **1978**, *48* (1), 117−126.
(28) McInerney, E. J.; Flinn, P. A. Diffusivity of Moisture in Thin Films. *20th International Reliability Physics Symposium* **1982**, 264−267.
(29) Stoney, G. G.; Parsons, C. A. The Tension of Metallic Films Deposited by Electrolysis. *Proceedings of the Royal Society of London. Series A, Containing Papers of a Mathematical and Physical Character* **1909**, *82* (553), 172−175.
(30) Lee, H.; Wong, S. S.; Lopatin, S. D. Correlation of Stress and Texture Evolution during Self- and Thermal Annealing of Electroplated Cu Films. *J. Appl. Phys.* **2003**, *93* (7), 3796−3804.
(31) Wu, W.-Q.; Yang, Z.; Rudd, P. N.; Shao, Y.; Dai, X.; Wei, H.; Zhao, J.; Fang, Y.; Wang, Q.; Liu, Y.; Deng, Y.; Xiao, X.; Feng, Y.; Huang, J. Bilateral Alkylamine for Suppressing Charge Recombination and Improving Stability in Blade-Coated Perovskite Solar Cells. *Sci. Adv.* **2019**, *5* (3), eaav8925.
(32) Glushkova, A.; Mantulnikovs, K.; Giriat, G.; Semeniuk, K.; Forró, L.; Horváth, E.; Arakcheeva, A. Effect of Thermal Cycling on the Structural Evolution of Methylammonium Lead Iodide Monitored around the Phase Transition Temperatures. *Solar RRL* **2019**, *3* (7), 1900044.
(33) Hu, Y.; Zhang, Z.; Mei, A.; Jiang, Y.; Hou, X.; Wang, Q.; Du, K.; Rong, Y.; Zhou, Y.; Xu, G.; Han, H. Improved Performance of Printable Perovskite Solar Cells with Bifunctional Conjugated Organic Molecule. *Adv. Mater.* **2018**, *30* (11), 1705786.
(34) Gutwald, M.; Rolston, N.; Printz, A. D.; Zhao, O.; Elmaraghi, H.; Ding, Y.; Zhang, J.; Dauskardt, R. H. Perspectives on Intrinsic Toughening Strategies and Passivation of Perovskite Films with Organic Additives. *Sol. Energy Mater. Sol. Cells* **2020**, *209*, No. 110433.
(35) Lan, Y.; Wang, Y.; Song, Y. Efficient Flexible Perovskite Solar Cells Based on a Polymer Additive. *Flexible and Printed Electronics* **2020**, *5* (1), No. 014001.
(36) Zhang, F.; Zhu, K. Additive Engineering for Efficient and Stable Perovskite Solar Cells. *Adv. Energy Mater.* **2020**, *10* (13), 1902579.
(37) Li, Y.; Dailey, M.; Lohr, P. J.; Printz, A. D. Performance and Stability Improvements in Metal Halide Perovskite with Intralayer Incorporation of Organic Additives. *J. Mater. Chem. A Mater.* **2021**, *9* (30), 16281−16338.
(38) Kim, H.; Figueroa Morales, C. A.; Seong, S.; Hu, Z.; Muyanja, N.; Penukula, S.; Zheng, T.; Pizzo, Z.; Yim, C. S.; Lenert, A.; Rolston, N.; Gong, X. Molecular Design of Defect Passivators for Thermally Stable Metal-Halide Perovskite Films. *Matter* **2024**, *7* (2), 539−549.
(39) Li, Y.; Lohr, P. J.; Segapeli, A.; Baltram, J.; Werner, D.; Allred, A.; Muralidharan, K.; Printz, A. D. Influence of Halides on the Interactions of Ammonium Acids with Metal Halide Perovskites. *ACS Appl. Mater. Interfaces* **2023**, *15* (20), 24387−24398.
(40) Jariwala, S.; Sun, H.; Adhyaksa, G. W. P.; Lof, A.; Muscarella, L. A.; Ehrler, B.; Garnett, E. C.; Ginger, D. S. Local Crystal Misorientation Influences Non-Radiative Recombination in Halide Perovskites. *Joule* **2019**, *3* (12), 3048−3060.
(41) Wang, H.; Zhu, C.; Liu, L.; Ma, S.; Liu, P.; Wu, J.; Shi, C.; Du, Q.; Hao, Y.; Xiang, S.; Chen, H.; Chen, P.; Bai, Y.; Zhou, H.; Li, Y.;

https://doi.org/10.1021/acsenergylett.4c00587
ACS Energy Lett. 2024, 9, 2101−2108

Chen, Q. Interfacial Residual Stress Relaxation in Perovskite Solar Cells with Improved Stability. *Adv. Mater.* **2019**, *31* (48), 1904408.
(42) Presnyakov, V. V.; Galstian, T. V. Electrically Tunable Polymer Stabilized Liquid-Crystal Lens. *J. Appl. Phys.* **2005**, *97* (10), No. 103101.
(43) Mazur, A. V.; Stepanova, L. P. Influence of Temperature on the Coefficient of Thermal Expansion of Monocrystals of Silicon. *Materials Science* **2005**, *41* (4), 531−537.
(44) Jacobsson, T. J.; Schwan, L. J.; Ottosson, M.; Hagfeldt, A.; Edvinsson, T. Determination of Thermal Expansion Coefficients and Locating the Temperature-Induced Phase Transition in Methylammonium Lead Perovskites Using X-Ray Diffraction. *Inorg. Chem.* **2015**, *54* (22), 10678−10685.
(45) Dai, Z.; Doyle, M. C.; Liu, X.; Hu, M.; Wang, Q.; Athanasiou, C. E.; Liu, Y.; Sheldon, B. W.; Gao, H.; Liu, S.; Padture, N. P. The Mechanical Behavior of Metal-Halide Perovskites: Elasticity, Plasticity, Fracture, and Creep. *Scr Mater.* **2023**, *223*, No. 115064.
(46) Layek, M.; Yang, I. S.; Dai, Z.; Ranka, A.; Cai, T.; Sheldon, B. W.; Chason, E.; Padture, N. P. Elastic Modulus of Polycrystalline Halide Perovskite Thin Films on Substrates. *arXiv:2307.07071* **2023**, DOI: 10.48550/arXiv.2307.07071v3.
(47) Lagrange, S.; Brongersma, S. H.; Judelewicz, M.; Saerens, A.; Vervoort, I.; Richard, E.; Palmans, R.; Maex, K. Self-Annealing Characterization of Electroplated Copper Films. *Microelectron. Eng.* **2000**, *50* (1), 449−457.
(48) Park, S. M.; Abtahi, A.; Boehm, A. M.; Graham, K. R. Surface Ligands for Methylammonium Lead Iodide Films: Surface Coverage, Energetics, and Photovoltaic Performance. *ACS Energy Lett.* **2020**, *5* (3), 799−806.
(49) van Franeker, J. J.; Hendriks, K. H.; Bruijnaers, B. J.; Verhoeven, M. W. G. M.; Wienk, M. M.; Janssen, R. A. J. Monitoring Thermal Annealing of Perovskite Solar Cells with In Situ Photoluminescence. *Adv. Energy Mater.* **2017**, *7* (7), 1601822.

https://doi.org/10.1021/acsenergylett.4c00587
ACS Energy Lett. 2024, 9, 2101−2108